

A Theoretical Model of Pattern Formation in Coral Reefs

Susannah Mistr and David Bercovici*

Department of Geology and Geophysics, School of Ocean and Earth Science and Technology, University of Hawaii, Honolulu, Hawaii 96822, USA

ABSTRACT

We present a mathematical model of the growth of coral subject to unidirectional ocean currents using concepts of porous-media flow and nonlinear dynamics in chemical systems. Linear stability analysis of the system of equations predicts that the growth of solid (coral) structures will be aligned perpendicular to flow, propagating against flow direction. Length scales of spacing between structures are selected based on chemical reaction and flow rates. In the fully nonlinear system, autocatalysis in the chemical reaction accelerates growth. Numerical

analysis reveals that the nonlinear growth creates sharp fronts of high solid fraction that, as predicted by the linear stability, advance against the predominating flow direction. The findings of regularly spaced growth areas oriented perpendicular to flow are qualitatively supported on both a colonial and a regional reef scale.

Key words: coral reefs; pattern formation; self-organization; colonial organisms.

INTRODUCTION

Coral reefs are composed of small, calcifying coral polyps that together build complex architectures. That these architectures can be different for colonies of the same species in different environmental conditions suggests that quantifiable, nongenetic chemical and physical controls are important in the organization of the system. **Although the complex interactions controlling the chemistry of coral calcification are difficult to model, it is possible to model some aspects of growth using fundamental principles of physics and chemistry.** **Important factors in the growth of coral include light, which influences the rate of calcification, and flow, which influences the delivery and uptake of the nutrients essential for growth.**

Herein we consider the simplest examples of

coral colonies and reef systems subject to one-dimensional nutrient-transporting water currents and construct a theoretical model of coral growth. **We simplify the growth process to a hypothetical chemical reaction between a limiting nutrient supplied by the water column and solid material manifest as a porous skeleton.** The chemical reaction, represented mathematically using the law of mass action, produces additional solid matrix. The self-enhancing growth of the solid matrix is said to be autocatalytic and reflects the need for an existing organism in order to sustain growth. The density of solid matrix influences the flow of the nutrient-bearing current by changing the constriction and/or tortuosity of fluid pathways or by inducing subcritical turbulence by means of enhanced surface roughness. Overall, we assume that an increase in matrix density impedes flow, creating a nonlinear feedback mechanism between matrix growth and nutrient supply. To consider how natural patterns may arise, we consider the behavior of perturbations in an initially uniform model system.

Alan Turing was one of the first to describe a theory for the onset of biological form and to consider theoretically the dynamics of spatially varying

Received 1 October 2001; accepted 22 May 2002.

*Corresponding author's current address: Department of Geology and Geophysics, Yale University, PO Box 208109, New Haven, Connecticut 06520-8109, USA; email: david.bercovici@yale.edu

Current address for S. Mistr: College of Medicine, Medical University of South Carolina, 96 Jonathan Lucas Street, PO Box 250617, Charleston, South Carolina 29425, USA

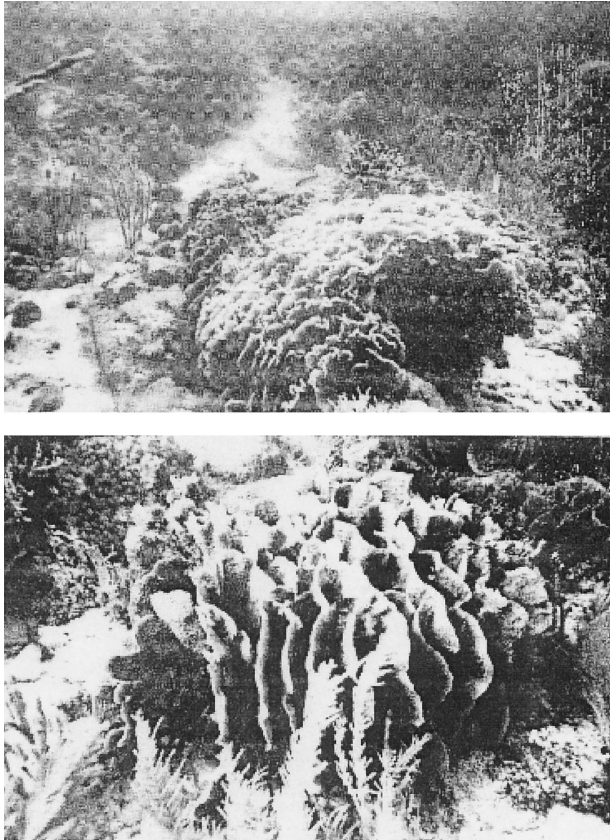


Figure 1. Aggregations of common reef coral *Agaricia tenuifolia*, Carrie Bow Cay, Belize. The colony consists of a series of upright plates oriented perpendicular to flow. The sand channel is parallel to the flow direction (after Helmuth and others 1997).

nonlinear chemical systems (Turing 1952). The key point in Turing's work relevant to many aspects of pattern formation is that asymmetry could be amplified by means of competing chemical reactions, and, as mitigated by diffusion, the asymmetry could be spatially distributed. By considering autocatalytic, or self-enhancing, chemical species Turing was able to show how steep gradients could result from a small perturbation to uniform concentrations.

Patterns in coral reefs range from the small-scale architecture of a particular colony to large-scale reef distribution patterns. Because of the many complex factors that can contribute to the development of these patterns, examples for theoretical study are taken from environments where one particular environmental parameter appears to play a distinctly significant role. In particular, the influence of ocean currents appears to affect coral reef orientation over many scales. On the colony scale, certain coral colonies orient as a series of plates perpendicular to the predominating direction of flow (Figure 1). On the



Figure 2. Bunker Reef group, Great Barrier Reef, Australia (after Jupp and others 1985).

regional scale, reef islands orient in series (Figure 2) along the predominating direction of large-scale currents (Figure 3).

Well-developed coral reefs are thought to be present in otherwise low-productivity waters due to the tight recycling of nutrients between symbiotic zooxanthellae within the tissues of the coral organism and the coral organisms themselves (Lewis 1973). Classically, these photosynthetic zooxanthellae provide oxygen and food for the coral organism through photosynthesis, while the coral in turn provides essential nutrients to the zooxanthellae through metabolic waste (Muscatine 1973). Calcification can be positively correlated with light exposure, indeed calcification rates can be about three times faster in light than in dark (Kawaguti and Sakumoto 1948; Baker and Weber 1975a, b; see also Gattuso and others 1999). It is therefore widely suspected that the photosynthesis in zooxanthellae contributes to increased rates of calcification. For a basic understanding of how photosynthesis may enhance calcification, we consider the overall reactions of both.

For photosynthesis, carbon dioxide (CO_2) and water (H_2O) are used to produce glucose and oxygen:



For calcification, calcium and bicarbonate ions pre-

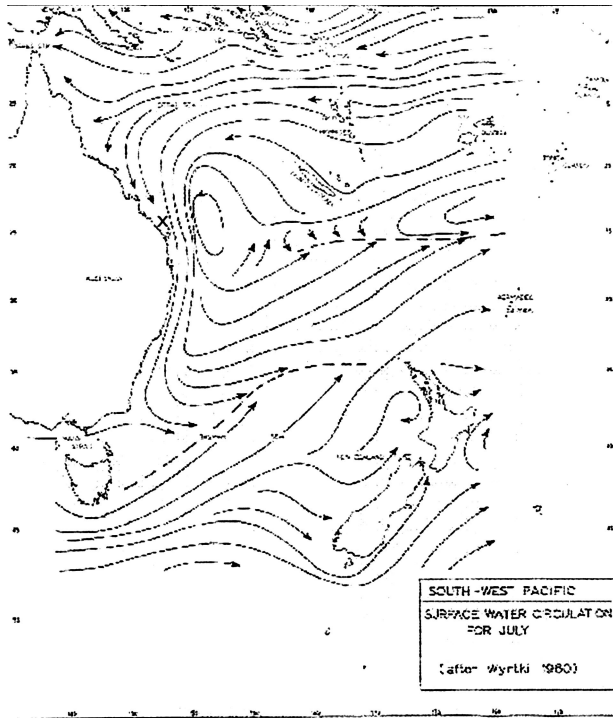
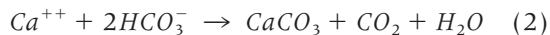


Figure 3. Southwest Pacific Circulation (after Maxwell 1968). "X" denotes the location of the Bunker Reef Group.

cipitate calcium carbonate and evolve carbon dioxide (Ware and others 1991, from Stumm and Morgan 1981):



The calcification reaction produces carbon dioxide, which can be used in photosynthesis. This removal of carbon dioxide by photosynthesis provides a mechanism by which the calcification reaction in Eq. (2) can be driven toward the right; it has been proposed that this mechanism explains enhanced calcification (Goreau 1963). Although this is a viable mechanism, the details of calcium supply and bicarbonate usage are poorly constrained; therefore, few conclusions can be drawn as to the significance of these reactions alone in enabling organismal calcification.

For example, complicating the simple photosynthesis-driven calcification hypothesis, some species of coral possess an organic matrix on the outside of cells lining the skeleton that contains calcium-binding substances (Isa and Okazaki 1987). The organic matrix provides a way to lower the energy for precipitation and thus drive calcification (Borowitzka 1987). Additionally, there is evidence that the incorporation of calcium into the coral skeleton is a

cellularly controlled process that requires metabolic energy for the pumping of materials into or out of the cell (see Gattuso and others 1999). Finally, the introduction of a mineral inhibitor can hold calcification to 1% of normal incorporation of calcium into the skeleton without affecting rates of photosynthesis (see Gattuso and others 1999).

The combination of these observations suggests that photosynthesis-driven calcification involves more complex chemical schemes than Eqs. (1) and (2); however, since the aim of this paper is to consider the relationship of growth and shape of coral colonies in response to differing environmental factors, it is not entirely necessary to understand the explicit mechanism of calcification. What we must consider is that skeletogenesis is an active process that occurs in the presence of the organism, which must be supplied with some form of food or energy. Because corals are known to feed on zooplankton and remove food fragments from the water column (Yonge 1930; Porter 1976), we devise very simplified "calcification" reactions where preexisting calcium carbonate "reacts" with some limiting nutrient to produce more calcium carbonate, representing coral growth. The nutrient is supplied at the sea surface and diffuses or settles downward. We then consider the effect of currents circulating through the reef by imposing a unidirectional flow on the system.

An interesting characteristic of coral reef morphology is that there is often a strong pattern of vertical zonation along the reef (see Jackson 1991). The absorption of light as it penetrates through the water column and the change in flow regime are suspected to contribute to the change of dominating form with depth (Baker and Weber 1975a, b; Graus and Macintyre 1989). Although the difference in dominating forms with depth is often related to a change in the dominating coral species and is thus more of an evolutionary problem, there are instances where corals of the same species exhibit morphological plasticity in accordance with flow regime. Using an example of *Pocillopora damicornis*, we see that as flow increases, morphology changes from more space-filling knobby forms in high-flow regimes to more delicately branching forms in low-flow regimes (Figure 4). Since the same species can exhibit different growth forms under different flow regimes, it is evident that the ambient environmental conditions profoundly influence morphology. The effect of water and nutrient flux in controlling biological pattern formation is obviously important in other environments as well, such as vegetation in semiarid areas (HilleRis-Lambers and others 2001).

It is our goal to understand how the calcification

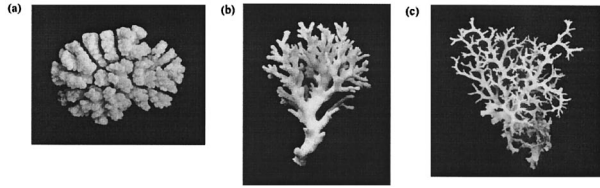


Figure 4. Three specimens of the coral *Pocillopora damicornis* from sites increasingly sheltered from water movement. Specimen a is most exposed to flow; specimen c is most protected from flow. After Kaandorp and others 1996 (from Veron and Pichan 1976).

rate and the flow regime affect the growth of coral reefs. We hypothesize that colonies and reefs develop their complex structures as they obstruct flow and intercept available nutrients, either by enhanced surface roughness or by increased complexity of the path for the flow field. Complex feedbacks among turbulent flow, nutrient supply, and calcification likely operate to generate the elaborate three-dimensional colony architectures. These complex interactions are unwieldy in theoretical continuum models and thus have largely been approached using idealized lattice Boltzman or cellular-automata models of aggregation to explain the increase of space-filling forms with increased flow regime (Preece and Johnson 1993; Kaandorp and others 1996).

Here we attempt to provide a simple, physically based model using basic carbonate chemistry in conjunction with a porous-flow model to describe the overall decrease in flow rate that accompanies the increase in coral cover that occurs as corals take nutrients from the water column. We represent increasing coral cover in the face of nutrient supply by the autocatalytic construction of a porous matrix infiltrated with fluid subject to a one-dimensional pressure gradient. The nutrient, supplied from the surface, diffuses through and is carried by the fluid. We arrive at the model by considering the conservation of mass for the fluid, dissolved nutrient, and the solid. We then analyze the model to explore the dynamic interaction of nutrient supply, solid and nutrient diffusion rates, flow rates, and chemical reaction rates and to find cases where small departures from the uniform system are amplified and patterning phenomena arise.

THEORETICAL MODEL

Although it is a simplification, considering that tissue, and thus growth, occurs only on the outer surface of the coral, we employ a porous-medium

formulation to model our skeletal framework. Making use of a porous matrix allows us to describe flow of fluid by Darcy's law in porous materials. Aharonov and others (1995) used a porous-medium formulation to address feedbacks between dissolution of host matrix and fluid infiltration for understanding melt-focusing beneath midocean ridges. Their model considered the interaction of dissolution, changing porosity, and enhanced fluid infiltration and revealed that larger channels develop at the expense of smaller channels, thus providing a mechanism for focusing melt beneath the ridge. The basic premise of their work is that changing porosity can affect flow velocity. This idea will be retained in our model; however, rather than considering a positive feedback between infiltration and dissolution, we examine the interaction of the autocatalytic growth of the matrix and the advective supply of a limiting nutrient.

The model system is considered to take place in a layer of thickness H that rests atop the sea floor but above which no coral grows (Figure 5). The coral reef mass is considered to be a porous, immobile, and solid matrix that reacts chemically with dissolved nutrient to form more solid matrix. The nutrient itself is supplied by a uniform source from the overlying water column and by flux of the nutrient-bearing water, forced to flow horizontally through the solid matrix by an imposed pressure gradient. The solid matrix has molar concentration ψ (that is, moles in a unit volume containing solid, fluid, and nutrient); the nutrient has molar concentration α . Both values are given in units of mol/m^3 to facilitate the provisions of a stoichiometric relation for their chemical reaction (see Appendix 1). The pressure whose gradient drives flow is denoted by P and has units of Pa. All three dependent variables (ψ , α , and P) change in space and time and obey equations of mass conservation and fluid flow (Darcy's law); however, these equations are vertically averaged in z so that they can be posed in terms of horizontal position (x, y) only, as well as time t (see Appendix 1).

The growth, loss, and transport of the nutrient is determined by its advective flux with water through the solid matrix, its diffusion through the water, and the mass lost through chemical reaction with the solid matrix; when all dependent and independent variables are nondimensionalized by the natural mass, length, time, and molar scales of the system (see Appendix 1), this relation is expressed as:

$$\frac{\partial \alpha}{\partial t} - \nabla_h \cdot [(1 - \psi)^2 \alpha \nabla_h P] = \nabla_h^2 \alpha + \alpha_s - \alpha - \beta \alpha \psi^2 \quad (3)$$

where ∇_h is the horizontal gradient operator, α_s is the uniform supply of nutrient through the top surface of the layer, and β is a chemical reaction parameter (that is, the dimensionless number that contains the reaction rate; see Appendix 1). The terms on the left side of Eq. (3) are (from left to right) the growth rate of nutrient density and the advective nutrient flux carried by Darcy flow that is itself forced by a pressure gradient $\nabla_h P$ through a matrix with permeability proportional to $(1 - \psi)^2$ (such that when the solid density $\psi = 1$, the matrix is impermeable). The terms on the right side represent horizontal diffusion of nutrient ($\nabla_h^2 \alpha$), vertical diffusion relative to the overlying source concentration ($\alpha_s - \alpha$, such that if $\alpha < \alpha_s$ nutrient diffuses down into the layer, and if $\alpha > \alpha_s$ it diffuses up out of the layer), and mass loss due to chemical reaction (term proportional to β). A coefficient of diffusivity for α does not explicitly appear in Eq. (3) because it is absorbed into the nondimensionalizing time scale (see Appendix 1).

The equation for change of solid matrix concentration is controlled only by mass addition through chemical reaction with nutrients and by loss through minor diffusion; such solid diffusion is used to represent both slight dissolution of coral reef mass and—perhaps more importantly—erosion and damage near the perimeter of coral reef concentrations, which are here represented as steep gradients in ψ . This leads to the following equation (again dimensionless):

$$\frac{\partial \psi}{\partial t} = \lambda \nabla_h^2 \psi - \lambda \psi + \beta \alpha \psi^2 \quad (4)$$

where λ is the solid matrix diffusivity (scaled by the nutrient diffusivity) and will be referred to as “the diffusion parameter” (see Appendix 1 for more details). The terms in Eq. (4) show growth of solid concentration (left side), diffusion both horizontally and vertically (terms proportional to λ), and mass addition from chemical reactions with the nutrient (term proportional to β).

Lastly, the mass conservation of water flowing through the matrix leads to an equation for pressure itself:

$$\nabla_h^2 P = \frac{2 \nabla_h \psi \cdot \nabla_h P}{(1 - \psi)} - \frac{1}{(1 - \psi)^2} \frac{\partial \psi}{\partial t} \quad (5)$$

where spatial adjustments in pressure (left side of the equation) are controlled by flow through constrictions in the matrix—for example, a “nozzle” effect (first term on right side) and a growth of the matrix that would squeeze fluid out of pores (last term on the right side).

Eqs. (3), (4), and (5) are the dimensionless governing equations that we use to analyze the stability of our autocatalytic, nutrient-limited porous matrix. The complete derivation of these equations and details about nondimensional parameters and nondimensionalizing scales are discussed in Appendix 1.

ANALYSIS OF THEORETICAL MODEL

Stability Analysis

Philosophy. One of the most powerful tools for elucidating self-organization and pattern formation in natural systems is *linear stability analysis*. Most systems have a simple equilibrium state that is essentially uniform and patternless. However, this equilibrium state might be unstable, so that disturbances or perturbations would grow and force the system to a different state with some inherent pattern. A ball atop a hill is a simple zero-dimensional example: Undisturbed, the ball can be balanced and remains at rest; but with a sufficient disturbance (for example, wind, earthquake, a light kick), the ball will roll off the hill and not stop until it reaches some other equilibrium state (for example, a valley deep enough to capture it).

The classic paradigm of instability and pattern formation in physics is that of thermal convection, whereby a fluid layer is uniformly heated along its base and cooled along its top. This system has a static and patternless thermally conductive state whereby heat is transported from the hot base to a cooler surface by transmission of molecular vibrations, or *phonons*. But since fluid near the hot base is less dense than fluid near the colder top, it is gravitationally unstable. Thus, perturbations or disturbances such as slight fluid motion can jostle the system and initiate overturn such that light fluid moves to the top and heavy fluid moves to the bottom; with the continuous heat supply through the bottom and heat loss through the top, the motion persists as convective circulation. The perturbation of a given length scale that can cause the layer to turn over most efficiently, or for the least amount of heat input, is generally the one that will grow the fastest and dominate the pattern of convection (that is, it will determine the length scale of the convection cells).

Thus, in stability analysis, one seeks the characteristics (length scale and temporal behavior, such as growth and propagation) of this dominant perturbation. The formalism of stability analysis is well explained in various texts (see, for example, Chandrasekhar 1961; Drazin and Reid 1989; Nicolis 1995). Here we employ the principles of linear sta-

bility analysis to build a framework for interpreting pattern formation and self-organization in our model coral reef system (see Appendix 2 for full details).

Equilibrium States. Given the cubic nonlinearity of the system of governing equations (in particular, the reaction term proportional to β in Eqs. [3] and [4]), there are three uniform equilibrium states. One such state is the trivial state, wherein there is no solid mass; the two other states involve small solid-mass fraction and large solid-mass fraction, respectively. The trivial state is stable and does not lead to any pattern formation, implying that at least some minimal amount of initial solid is necessary to initiate instability and pattern growth; hence, we do not consider this state further. Likewise, the high solid fraction state is stable under almost all conditions and is also not very susceptible to pattern formation, implying that little more solid structure can be built if the solid fraction is near its maximum allowed value; we will therefore not consider this state either. (For discussion of these states, see Appendix 2.)

The low solid fraction state is unstable to perturbations and leads to the growth of structures. This state is denoted by (ψ_0, α_0, P_0) where:

$$\psi_0 = \frac{1}{2} \left(\frac{\alpha_s}{\lambda} - \sqrt{\frac{\alpha_s^2}{\lambda^2} - \frac{4}{\beta}} \right), \quad \alpha_0 = \alpha_s - \lambda \psi_0 \quad (6)$$

and the equilibrium pressure has a constant gradient given $dP_0/dx = -v$, which represents an imposed background current velocity or flow rate. (Note that in Appendix 2, this equilibrium state is referred to by ψ_0^- to keep it distinct from the other equilibrium states; here we drop the “−” superscript.)

Instability of Perturbations. We next address the question of perturbations to the equilibrium state given by Eq. (6) and consider how their properties (growth rate, spatial structure) are affected by the model parameters. To maintain a manageable parameter space, we examine only the effect of varying the flow rate v and reaction rate β , and we hold solid diffusion fixed at $\lambda = 10^{-3}$ (that is, much smaller than nutrient diffusion) and surface nutrient supply fixed at $\alpha_s = 9 \times 10^{-4}$ (much smaller than the molar concentration of pure solid by which all molar concentrations have been nondimensionalized; see Appendix 1).

As shown in Appendix 2, the only perturbations that grow are completely uniform in the y (cross-current) direction and have nonuniform structure in the x (along-current) direction. We therefore only need to consider the x and t (time) dependence

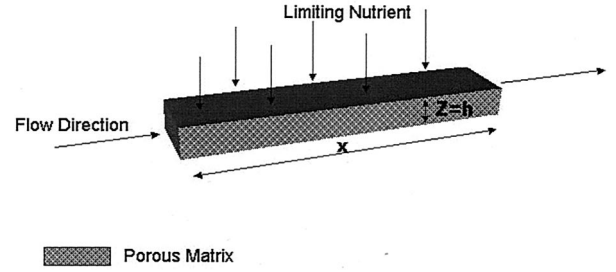


Figure 5. Schematic of the model. Fluid infiltrates the porous matrix, and flow is maintained by a pressure gradient in one direction. Limiting nutrient is supplied from the surface, diffuses through the fluid, and reacts with the matrix for the autocatalytic production of additional matrix. The model assumes that the system is continuous in x and y with finite depth $z = H$.

of our system instead of the x , y , and t dependence. We thus assume that each perturbation to ψ_0 , α_0 , and P_0 is a sinusoid in x , with wavenumber k (that is, wavelength $2\pi/k$) and growth rate s . The growth rate s can be complex; the real part $Re(s)$ implies growth (if positive) or decay (if negative), while the imaginary part $Im(s)$ implies wavelike propagation. (As shown in Appendix 2, there are in fact two possible growth rates for each k , although only one allows growth of perturbations; this growth rate is referred to in Appendix 2 as s_+ , but for simplicity we have dropped the “+” subscript here; however, in all the figures, we still refer to s_+ for consistency with the figures in the appendices.)

If we consider an infinite number of perturbations with different wavelengths, the one that has the largest growth rate $\max(Re(s))$ will dominate the pattern that evolves. The wavelength of this fastest growing perturbation is $2\pi/k_{max}$, and its propagation rate, or wavespeed, is:

$$c_{max} = -Im(s)_{max}/k_{max} \quad (7)$$

where $Im(s)_{max}$ is the imaginary part of s whose real part is $\max(Re(s))$.

Figure 6 shows the maximum growth rate $\max(Re(s))$ along with the corresponding wavenumber k_{max} and wavespeed c_{max} as functions of flow velocity v and for three reaction rates $\beta = 5, 10$, and 100 . The maximum growth rate increases monotonically with both v and β (Figure 6a), although for the large reaction rate $\beta = 100$, the growth rate is nearly constant over v . Because $\beta = 100$ corresponds to a very fast chemical reaction, there is little influence from current velocity since the reaction is nearly instantaneous for any flow rate. On the other hand, for slower reactions, such

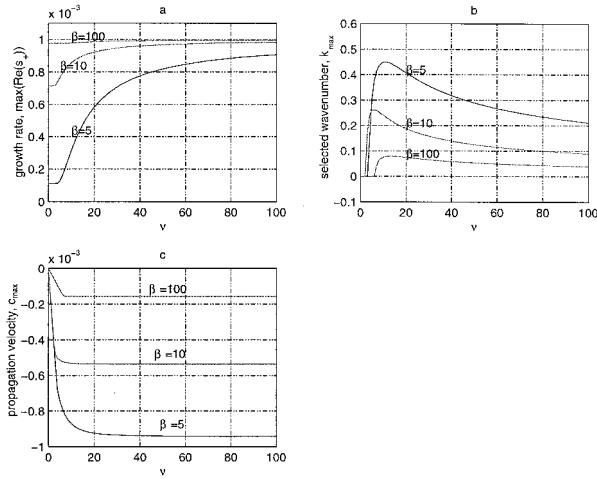


Figure 6. Maximum growth rate $\max(\text{Re}(s_+))$ of least stable perturbation (a), corresponding wavenumber k_{\max} (where perturbation wavelength is $2\pi/k$) (b), and corresponding propagation velocity $c_{\max} = -\text{Im}(s_+)/k$ (c) as functions of imposed flow velocity (or pressure gradient), v , for three reaction rates, $\beta = 5$, $\beta = 10$, and $\beta = 100$.

as $\beta = 5$, we see increased growth rates as the flow speed increases, suggesting that the growth of solid structures is more sensitive to nutrient supply from the current for slower chemical reaction rates. As $v \rightarrow \infty$, the growth rates for $\beta = 5$ approach those for $\beta = 10$ and 100 as the growth rate of the dominant perturbation becomes primarily controlled by the nutrient flux from the moving current.

This one-dimensional model also reveals that the system develops solid growth maxima at characteristic, finite wavelengths ($2\pi/k_{\max}$) over a wide range of v and β (Figure 6b). For zero fluid flow, $v = 0$, spatial variability leads only to diffusive loss and thus decay of perturbations to the solid and nutrient fields; therefore, the wavelength or spacing for the fastest-growing structure is infinite ($k_{\max} = 0$) for all β —that is, growth is spatially uniform with no fluid motion. However, as the background flow speed is increased ($v > 0$), nutrient parcels become depleted asymmetrically as upstream reaction affects downstream supply; thus, a finite wavelength or spacing for fastest-growing patterns occurs. However, the wavelength of the fastest-growing structures at first decreases (k_{\max} increases) with increasing flow v ; then, at a critical v , it increases again (Figure 6b), which suggests competition between effects. In particular, a decrease in wavelength with increased flow permits sharper pressure gradients with which to impede flow and more efficiently capture nutrients; however, at too sharp a wavelength, the growth of structures is limited by diffu-

sion (as occurs in many classic problems of diffusion-limited aggregation [DLA]). Beyond the critical v , diffusion destroys the advantage of having sharp pressure gradients and thus the system's dominant length scale becomes determined by the recovery length—that is, the distance traveled by a nutrient-depleted parcel of fluid before it recovers its nutrient content via the surface supply α_s ; this recovery distance is obviously influenced by the fluid velocity, as demonstrated in Figure 6b. In this latter regime (that is, for v greater than the critical value), increased reaction rates (larger β) also cause the spacing of structures to grow (k_{\max} decreases) because the fast reaction depletes the nutrients more thoroughly and rapidly, necessitating a longer recovery.

Our model also shows that fastest-growing perturbation also propagates into the incoming flow ($c_{\max} < 0$). By supplying more abundant nutrients upstream, increasing v drives the system toward upstream growth—that is, the structure propagates toward the upstream accumulation fronts (for example, the direction a surface travels while being, in effect, spray-painted). As v affects the nutrient supply, it affects the slowest reaction cases the most—that is, those with small β —since for fast reactions, nutrients stay more ubiquitously depleted. A constant propagation value is achieved at a critical flow rate v , since, above a certain flow rate, the nutrient supply must still be affected by the rate at which it is supplied by nutrients from the surface.

The important features of this linear stability analysis predict that perturbations to our nonlinear system will grow, and that the system will be characterized by the development of gradients in the solid and nutrient fields that propagate upstream.

Nonlinear Analysis

For the nonlinear analysis, we build on the results from the linear stability analysis. We assume that derivatives in y are zero for Eqs. (3), (4), and (5), thus effectively considering the evolution of the one-dimensional nonlinear system.

We integrate the nonlinear equations using finite differences. We take the fully explicit forward-time difference for time derivatives and a space-centered difference for second-order derivatives; for first-order spatial derivatives, which reflect advection, we use upwind-differencing (Jain 1984; Press and others 1992). The Courant condition on the time-differencing is met by time-stepping at 10% of the Courant time-step (Press and others 1992). For the evaluation of the pressure field, we assume an instantaneous response to changed solid and nutrient

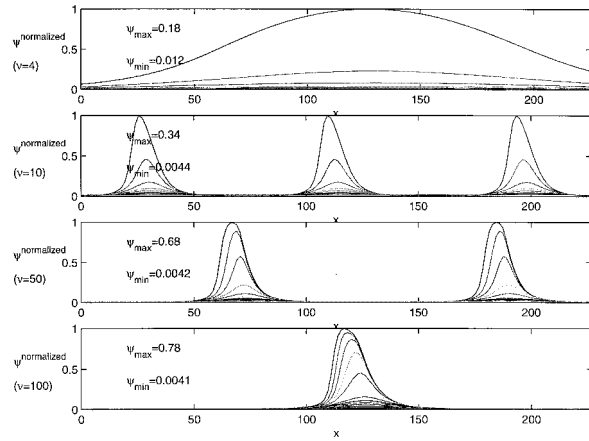


Figure 7. Solutions for ψ , the solid matrix, versus x for the time integration of the nonlinear system for perturbations to the steady state for $\beta = 100$. Contours represent different stages in the time evolution; the maximum amplitudes reflect the most recent time integration and are approximately evenly spaced in time. The indicated peak and trough values of ψ , ψ_{\max} , and ψ_{\min} are for the first and last contour, and $\psi^{\text{normalized}} = (\psi - \psi_{\min}) / (\psi_{\max} - \psi_{\min})$. From top to bottom, solutions for slow flow ($\nu = 4$), moderate flow ($\nu = 10$), high flow ($\nu = 50$), very high flow ($\nu = 100$). Perturbations to the steady state were at the wavelength of the least stable mode predicted by the linear stability analysis at 10% of the steady-state value $\psi_0 = 0.0113$; however, the magnitude of the perturbation for the $\nu = 4$ case is 1% of ψ_0 .

fields. We solve for P at each grid point using a tridiagonal matrix solver (Press and others 1992). We then use the adjusted pressure field in the next time-step integration of the nutrient and solid fields. Convergence tests and comparisons with linear stability analytic solutions suggest that the division of the domain into 201 grid points provides sufficiently precise solutions.

Because the system is open, we expect the nutrient and solid fields to obey Eqs. (3), (4), and (5) at the boundaries. The first derivatives of pressure, P , at the endpoints are approximated by making use of the second-order Taylor expansions of the two points interior to the boundary, expanded around the boundary itself. For the nutrient α and solid ψ , derivative expressions are approximated by the derivatives of the nearest interior point. Because we cannot specify α and ψ at the endpoints, we cannot make use of the Taylor expansion about the boundaries, as in the case of pressure.

Since there are an infinite number of nonlinear solutions, here we seek only to extend the results of the linear stability analysis into the nonlinear regime. Thus, we consider small perturbations to the

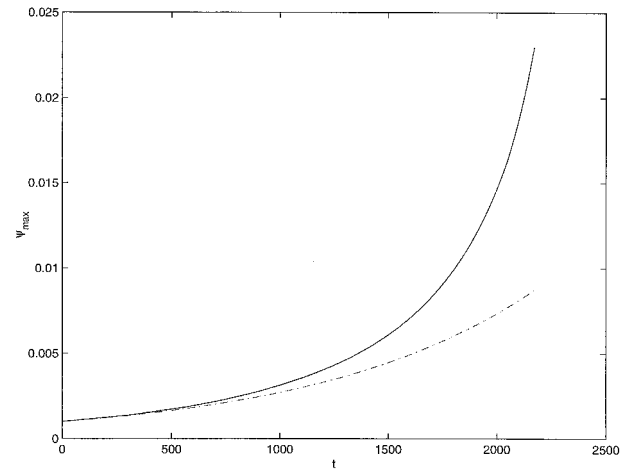


Figure 8. Values of ψ , the solid matrix, versus time t for linear stability solution for perturbations to ψ_0 (dashed line) and for nonlinear solutions (solid line) after 2800 time steps. Result is for perturbations to the steady state for $\beta = 100$, $\nu = 100$.

uniform steady state, ψ_0 (Eq. [6]), as in the linear stability analysis. We assume the steady state of the system is perturbed at 10% of the steady-state value, and we integrate the equations over time. We assume that the system selects the scale predicted by the linear stability, and we perturb the system at that selected wavelength.

We show the results of the numerical integration of the nonlinear system for the fastest reaction rate β and for four different values of the pressure gradient ν , which is defined here, for our finite domain, as $\nu = (P_l - P_r)/X$, where X is the length of domain in x and P_l , P_r are the pressures at the left and right boundaries, respectively (in the cases considered here, $P_l > P_r$). In these numerical calculations, we consider how the nonlinearities in the autocatalysis affect the shape and propagation of an infinitesimal perturbation. For $\beta = 100$, the fastest reaction parameter examined, we show the development of solid growth fronts for a range of four flow parameters (Figure 7). These results show strong asymmetry between the peaks and troughs, suggesting that the autocatalysis in the chemical reaction acts to accelerate the growth of the solid maxima. With respect to the linear system, growth is greatly accelerated (Figure 8).

Examining the behavior of the associated nutrient fields for $\beta = 100$, $\nu = 50$ permits a good illustration of the system's behavior (Figure 9). Here we find that the sharply growing solid fronts deplete the nutrient field and that the downstream recovery of the nutrient field controls the spacing of the solid fronts. Also, we see that the fronts prop-

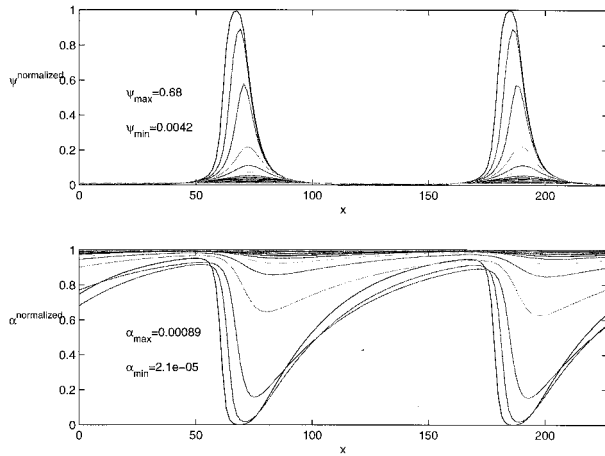


Figure 9. Normalized solutions for (from top to bottom) ψ , the solid matrix, and α , the nutrient field, versus x for the time integration of the nonlinear system for perturbations to the steady state for $\beta = 100$, $\nu = 50$. See Figure 7 for information about contours and normalization.

agate upstream. For the $\beta = 10$ and $\beta = 5$ cases the results are very similar, although growth is much slower and the asymmetry is not as extensively exaggerated by the end of the time integrations (Mistr 1999).

DISCUSSION OF THE MODEL

The main result from the nonlinear analysis is the development of pronounced nutrient and solid fronts that propagate upstream. Sharp gradients in the nutrient field develop as the solid depletes the available nutrient by reacting autocatalytically to create additional solid that can further deplete the nutrient. Growth of the solid due to the autocatalysis is greatly accelerated with respect to the linear system, and this rapid growth must far exceed diffusive loss to allow for the development of the solid fronts. These fronts are most pronounced for increased reactions rates and increased flow rates. We can conclude from this analysis that without the nonlinearities of the autocatalysis in the reaction chemistry, the development of sharp fronts is not possible. The self-enhancing behavior of the solid acts to deplete local nutrient concentrations sharply, so that growth occurs most rapidly in the upstream direction, where nutrient supply is greatest. To some extent, the solid structures act as nutrient filters; thus, it is not surprising that they accumulate and absorb nutrients faster on the supply side of the structures. The areas of high solid concentration act to impede flow, increasing the potential for nutrient depletion and further growth.

Spacing of the fronts is invariably controlled by the competition among (a) the propensity for solid structures to introduce sharp pressure gradients through obstructions that impede flow and thus more effectively capture nutrients; (b) the diffusion of sharp gradients in both the solid and (especially in the cases considered here) nutrient fields; and (c) both the decay and recovery length scales over which the nutrient content in a parcel of fluid is, while being swept downstream, either lost to reactions with the solid or replenished by surface supply.

We find that the slowest-reacting systems are the most sensitive to changes in the imposed fluid flow (or pressure gradient) in terms of the growth rates and selected wavelength for the growing structures (Figure 6a and b), suggesting that slow-growing corals are most susceptible to environmental plasticity. Also, we expect this plasticity to be the most evident over slow flow regimes. We further find that for the fastest reactions, as well as the fastest flow rates, long wavelengths dominate (Figure 6b), suggesting that faster-growing systems might exhibit broader structures.

As we have mentioned, there are morphologies of coral reefs that orient perpendicular to flow, with regular spacing of the growth plates parallel to flow (Figure 1). Our theory suggests that this type of reef is organizing to best intercept nutrient supply, whereas nonlinear growth permits the development of sharp growth fronts in the face of a one-dimensional flow. Additionally, the regular spacing of reef cays off the coast of Queensland parallel to the main direction of the East Australian Current leads us to anticipate a similar mechanism for reef organization (Figure 2). Evidence of upstream propagation in each of the colonial and large-scale cases is difficult to ascertain, although further investigation of these areas would reveal clues. Examining the paleohistory of Bunker Reef would help to establish the validity of the hypothesis of nutrient-controlled growth patterns. Additionally, it would be enlightening to determine whether *A. tenuifolia* advances into the flow as it grows additional plates. Because the nondimensional scales include hypothetical reaction components, it is not informative to consider the physical scaling of the spacing.

The model presented here is quite simplified, and thus many possibilities exist for further theoretical modeling of reef systems. As information comes to light regarding the relationship of photosynthesis to calcification, a simple model of the chemical dynamics of calcification would be very appropriate.

Appendix 1. Derivation of the Theoretical Model

Let us suppose a system wherein we have a porous matrix of solid material, ψ in $\text{mol} \cdot \text{m}^{-3}$, infiltrated with fluid containing dissolved nutrient α in $\text{mol} \cdot \text{m}^{-3}$. This dissolved nutrient undergoes a reaction with the solid material that generates additional solid material (Figure 5). In other words, the system is subject to the autocatalytic production of ψ . Stated symbolically;



with a rate constant, or activity coefficient, k , where units depend on the stoichiometric coefficients, l , m , and n , where $n = m + l$. The stoichiometric coefficients specify the number of $\text{mol} \cdot \text{m}^{-3}$ that react and are produced. The law of mass action states that the rate of a chemical reaction is proportional to the product of the concentrations of the reactants raised to their stoichiometric coefficients (Bailyn 1994; Nicolis 1995). In an ideal system, this rate would be given by the product of the number of moles per m^3 of the reactants alone, which gives the statistical probability of the two species coming into contact; however, in reality, a rate constant, or activity coefficient, such as k must be used as a proportionality factor to account for the gap between the statistical probability and the actuality of the reaction occurring (Nicolis 1995). To constrain the stoichiometric coefficients for the hypothetical reaction, we picked $l = 1$ for simplicity and investigated the stability of a system for various m and found that the system is unstable, yielding solid growth only in cases where $m \geq 2$ (Mistr 1999). We chose the lowest-order unstable case for our model, given by:



in which case k 's units are $\text{m}^6 \text{mol}^{-2} \text{s}^{-1}$. Thus, according to the law of mass action, for rate of change of fluid and solid material (with no flow or other sources of mass):

$$\left(\frac{\partial \alpha}{\partial t} \right)_{\text{reaction}} = -k\alpha\psi^2 \quad (\text{A3})$$

$$\left(\frac{\partial \psi}{\partial t} \right)_{\text{reaction}} = k\alpha\psi^2 \quad (\text{A4})$$

These two expressions provide the chemical source and sink terms for our model. We must consider

chemical diffusion and advection of mobile species and therefore make the following fundamental assumptions. First, we consider that the dissolved species (nutrients) do not contribute to the volume of the fluid infiltrating the porous matrix. Second, the solid is considered immobile (with respect to advection) although subject to diffusive loss.

Loss of solid mass is accounted for solely by effective diffusion of ψ representing, for example, disintegration and erosion near the perimeters of coral reef concentrations that are represented by sharp gradients in ψ ; thus, its time rate of change is:

$$\frac{\partial \psi}{\partial t} = D_\psi \nabla^2 \psi + k\alpha\psi^2 \quad (\text{A5})$$

We relate the velocity of the fluid to the evolving pressure gradient by Darcy's law (Bear 1988):

$$\mathbf{q} = -\frac{K_0(1 - \gamma\psi)^2}{\eta} \nabla P \quad (\text{A6})$$

where \mathbf{q} is the Darcy velocity vector, η is fluid viscosity, γ is the volume that one mole of pure solid occupies such that $1 - \gamma\psi$ is the matrix porosity, and $K_0(1 - \gamma\psi)^2$ is the porosity-dependent permeability in which K_0 is a reference permeability. Conservation of fluid mass (assuming the fluid is incompressible) prescribes that:

$$\frac{\partial}{\partial t} (1 - \gamma\psi) + \nabla \cdot \mathbf{q} = 0 \quad (\text{A7})$$

(see Mistr 1999; also Bercovici and others 2001 and references therein), which leads to:

$$\nabla^2 P = \frac{2\gamma}{1 - \gamma\psi} \nabla \psi \cdot \nabla P - \frac{\gamma\eta}{K_0(1 - \gamma\psi)^2} \frac{\partial \psi}{\partial t} \quad (\text{A8})$$

With an expression for the velocity of the fluid, we may then consider the evolution of the nutrient field. The time rate of change for the nutrient, α , is controlled by advection, diffusion, and reactive loss, leading to:

$$\frac{\partial \alpha}{\partial t} + \nabla \cdot (\mathbf{q}\alpha) = D_\alpha \nabla^2 \alpha - k\alpha\psi^2 \quad (\text{A9})$$

Our governing equations are (A5), (A6), (A8), and (A9), which interrelate advection of our nutrient to growth of the solid. We consider the system to be continuous horizontally, in x and y , with finite vertical thickness, H . We supply nutrient to the system by holding the nutrient density at the top surface constant, $\alpha = \alpha_s$ at $z = H$. Holding the left entrance to the channel ($x = 0$) at a constant pressure, P_l , and maintaining the right exit at a constant lower pressure, P_r , we force fluid in the x direction, al-

though the resulting flow with various obstructions due to heterogeneity in the matrix can be in any direction. To simplify the system to a two-dimensional model, we integrate the equations over the channel depth, z , assuming that vertical profiles of the solid and the nutrient are parabolic to first order in order to match the top and bottom boundary conditions. Thus, the nutrient concentration α is constrained at the top by the surface nutrient supply α_s , and changes parabolically to zero gradient at the bottom (that is, an effectively insulating bottom boundary through which neither flow nor particle diffusion can occur). The solid concentration ψ is held to zero at the top and increases parabolically to zero gradient at the bottom (again, the bottom is effectively insulating). From these boundary conditions we assume that:

$$\alpha(x, y, z, t) = \alpha_s + (\bar{\alpha}(x, y, t) - \alpha_s)f(z) \quad (\text{A10})$$

$$\psi(x, y, z, t) = \bar{\psi}(x, y, t)f(z) \quad (\text{A11})$$

where:

$$f(z) = \frac{3}{2} \left(1 - \frac{z^2}{H^2} \right) \quad (\text{A12})$$

and since $\frac{1}{H} \int_0^H f(z) dz = 1$, then $\bar{\alpha}$ and $\bar{\psi}$ are the values of α and ψ , respectively, averaged over z . Substituting the above functions into Eqs. (A5), (A6), (A8), and (A9), integrating in z , and eliminating q , we find:

$$\begin{aligned} \frac{\partial \bar{\alpha}}{\partial t} - \nabla_h \cdot \left(\bar{\alpha} \frac{K_0(1 - \gamma \bar{\psi})^2}{\eta} \nabla_h \bar{P} \right) \\ = D_\alpha \nabla_h^2 \bar{\alpha} + D_\alpha \frac{3(\alpha_s - \bar{\alpha})}{H^2} - k \bar{\alpha} \bar{\psi}^2 \end{aligned} \quad (\text{A13})$$

$$\frac{\partial \bar{\psi}}{\partial t} = D_\psi \nabla_h^2 \bar{\psi} - D_\psi \frac{3\bar{\psi}}{H^2} + k \bar{\alpha} \bar{\psi}^2 \quad (\text{A14})$$

$$\nabla_h^2 \bar{P} = \frac{2\gamma \nabla_h \bar{\psi} \cdot \nabla_h \bar{P}}{(1 - \gamma \bar{\psi})} - \frac{\gamma \eta}{K_0(1 - \gamma \bar{\psi})^2} \frac{\partial \bar{\psi}}{\partial t} \quad (\text{A15})$$

where ∇_h is the horizontal gradient. For nonlinear terms, we have assumed that $\frac{1}{H} \int_0^H f^m(z) dz \approx 1$ (where m is any integer), which is generally only true for $m \leq 3$; however, more accurate integration only introduces factors that are $O(1)$, which can be absorbed into the system by slightly redefining constants such as K_0 , k , and γ . Since the equations are made nondimensional anyway (see below), these factors have no effect on the final governing equa-

tions and merely change the dimensional scales of the system by a few tens of percent.

These equations are nondimensionalized according to natural length, time, mass, and molar scales, $L = \frac{H}{3^{1/2}}$, $T = \frac{H^2}{3D_\alpha}$, $M = \frac{\eta H^5}{3^{5/2} D_\alpha K_0}$, $N = \frac{H^3}{\gamma 3^{3/2}}$, respectively, resulting in (dropping the overbars for simplicity):

$$\frac{\partial \alpha}{\partial t} - \nabla_h \cdot [(1 - \psi)^2 \alpha \nabla_h P] = \nabla_h^2 \alpha + \alpha_s - \alpha - \beta \alpha \psi^2 \quad (\text{A16})$$

$$\frac{\partial \psi}{\partial t} = \lambda \nabla_h^2 \psi - \lambda \psi + \beta \alpha \psi^2 \quad (\text{A17})$$

$$\nabla_h^2 P = \frac{2 \nabla_h \psi \cdot \nabla_h P}{(1 - \psi)} - \frac{1}{(1 - \psi)^2} \frac{\partial \psi}{\partial t} \quad (\text{A18})$$

where:

$$\lambda = \frac{D_\psi}{D_\alpha} \quad (\text{A19})$$

$$\beta = \frac{k H^2}{3 \gamma^2 D_\alpha} \quad (\text{A20})$$

The first parameter, λ , is the ratio of diffusion coefficients of the solid to nutrient and will be referred to as “the diffusion parameter.” The second nondimensional parameter, which contains k , the rate constant of the reaction, will be called “the reaction parameter,” β .

Eqs. (A16), (A17), and (A18) are the dimensionless governing equations that we use to analyze the stability of our autocatalytic, nutrient-limited porous matrix; these equations are reproduced in the main text as Eqs. (3)–(5).

Appendix 2. Linear Stability Analysis

Here we consider the growth of perturbations to a spatially constant system, characterized by uniform distribution of solid and nutrient and an imposed, constant pressure gradient. For small perturbations, solutions take the form:

$$\alpha = \alpha_0 + \epsilon \alpha_1 \quad (\text{A21})$$

$$\psi = \psi_0 + \epsilon \psi_1 \quad (\text{A22})$$

$$P = P_0(x) + \epsilon P_1 \quad (\text{A23})$$

where $\epsilon \ll 1$. Substituting these solutions into the two-dimensional equations gives rise to the three steady-state equations $O(\epsilon^0)$:

$$\alpha_s - \alpha_0 = \beta \alpha_0 \psi_0^2 \quad (\text{A24})$$

$$\lambda \psi_0 = \beta \alpha_0 \psi_0^2 \quad (\text{A25})$$

$$\frac{d^2 P_0}{dx^2} = 0 \quad (\text{A26})$$

the solutions of which are the trivial case:

$$\psi_0^0 = 0, \alpha_0 = \alpha_s \quad (\text{A27})$$

and the two conjugate roots:

$$\psi_0^\pm = \frac{1}{2} \left(\frac{\alpha_s}{\lambda} \pm \sqrt{\frac{\alpha_s^2}{\lambda^2} - \frac{4}{\beta}} \right) \quad (\text{A28})$$

where for all solutions $\alpha_0 = \alpha_s - \lambda \psi_0$ and the 0th-order pressure gradient is $dP_0/dx = -\nu$, where ν is constant.

With pressure specifications, we have introduced a fourth parameter, ν , and thus fix two of the nondimensional parameters so as to maintain a manageable parameter space. We assume that the variation in the diffusion coefficients is minimal, such that the ratio of solid to nutrient diffusion, λ , remains constant. We fix $\lambda = 0.001$, corresponding to nutrient diffusion that is 1000 times faster than solid diffusion. Since the 0th-order porosity $1 - \psi_0$ must be between 0 and 1, then $0 \leq \psi_0 \leq 1$, thus demanding that $\alpha_s/\lambda < 1$, as well as that $\alpha_s^2\beta/(4\lambda^2) > 1$, to ensure real ψ_0 . Therefore, we set $\alpha_s = 0.0009$, which, recall, is nondimensionalized by the molar volume of the pure solid. Dimensionally, this is effectively a surface concentration of around 200 mol/m^3 , assuming solid density for the calcium carbonate skeleton to be around 2.5 g/cm^3 . Setting constant values for two of the parameters, α_s and λ , permits us to examine changes in the system as the background pressure gradient, ν , and the reaction parameter, β , are varied.

The trivial case (A27) implies that there is no matrix present and that the nutrient distribution matches the surface supply. The two quadratic roots, (A28), represent steady states characterized by either high (ψ_0^+) or low (ψ_0^-) solid density. The high solid-density steady state evolves when there is not enough nutrient to react and support growth beyond that which balances diffusive loss, whereas the low solid-density state evolves since there is not enough solid to react and sustain growth beyond that which is lost to diffusion.

The stability of each of the high- and low-density matrix steady states, as well as the trivial case, is examined using equations $O(\epsilon^1)$ from substitutions of solutions (A21), (A22), and (A23) into the two-dimensional Eqs. (3), (4), and (5):

$$\begin{aligned} \frac{\partial \alpha_1}{\partial t} + 2\alpha_0(1 - \psi_0)\nabla P_0 \cdot \nabla \psi_1 & \\ - (1 - \psi_0)^2 \nabla P_0 \cdot \nabla \alpha_1 - (1 - \psi_0)^2 \alpha_0 \nabla^2 P_1 & \\ = \nabla^2 \alpha_1 - \alpha_1 - 2\beta \alpha_0 \psi_0 \psi_1 - \beta \psi_0^2 \alpha_1 & \quad (\text{A29}) \end{aligned}$$

$$\frac{\partial \psi_1}{\partial t} = \lambda \nabla^2 \psi_1 - \lambda \psi_1 + 2\beta \alpha_0 \psi_0 \psi_1 + \beta \psi_0^2 \alpha_1 \quad (\text{A30})$$

$$\nabla^2 P_1 = \frac{2\nabla P_0 \cdot \nabla \psi_1}{(1 - \psi_0)} - \frac{1}{(1 - \psi_0)^2} \frac{\partial \psi_1}{\partial t} \quad (\text{A31})$$

We assume that solutions to the above equations take the form:

$$(P_1, \alpha_1, \psi_1) = (P_k, \alpha_k, \psi_k) e^{i\mathbf{k} \cdot \mathbf{r} + st} \quad (\text{A32})$$

where s is the growth/decay rate, $\mathbf{k} = (k_x, k_y)$ is the horizontal wavenumber vector, and $\mathbf{r} = (x, y)$ is the horizontal position vector. Assuming solutions of this type implies that for each wavenumber pair (k_x, k_y) there is an associated growth or decay rate. Since wavenumber is related to wavelength, establishing which wavenumber supports the fastest growth allows us to predict the spatial scale over which the solid field exhibits preferred growth.

Substituting perturbation solutions (A32) into Eqs. (A29), (A30), and (A31), we find the dispersion relation:

$$\begin{aligned} s^2 + s[(1 + \lambda)(1 + k^2) + \beta \psi_0(\psi_0 - 2\alpha_0 + \alpha_0 \psi_0) \\ + ik_x \nu(1 - \psi_0)^2] + (1 + k^2)[\lambda(1 + k^2) + \lambda \beta \psi_0^2 \\ - 2\beta \alpha_0 \psi_0] + ik_x \nu(1 - \psi_0)^2[\lambda(1 + k^2) - 2\beta \alpha_0 \psi_0] \\ = 0 \quad (\text{A33}) \end{aligned}$$

where $k^2 = k_x^2 + k_y^2$. Eq. (A33) has two complex roots, s_\pm (where the “ \pm ” subscript indicates the sign of the radical term in the quadratic formula solution), only one of which, s_+ , allows growth.

We explore the growth rates $Re(s_+)$ versus $\mathbf{k} = (k_x, k_y)$ over a wide range of the nondimensional parameters for the three steady states and find that in all cases, the maximum growth rate $max(Re(s_+))$ occurs for $k_y = 0$. As an example of this result, we show the growth rate $Re(s_+)$ versus $\mathbf{k} = (k_x, k_y)$ for one reaction parameter β over a range of pressure gradients, ν for the steady state ψ_0^- (A28) (Figure A1). We select ψ_0^- because growth is sustained for perturbations to this steady state, whereas growth is sustained for neither the trivial case ψ_0^0 nor for the high solid-mass concentration case ψ_0^+ over the wide range of parameters that were sampled. Here we see that the fastest growth rate for low solid-mass concentration case ψ_0^- occurs at $k_x \neq 0$ and k_y

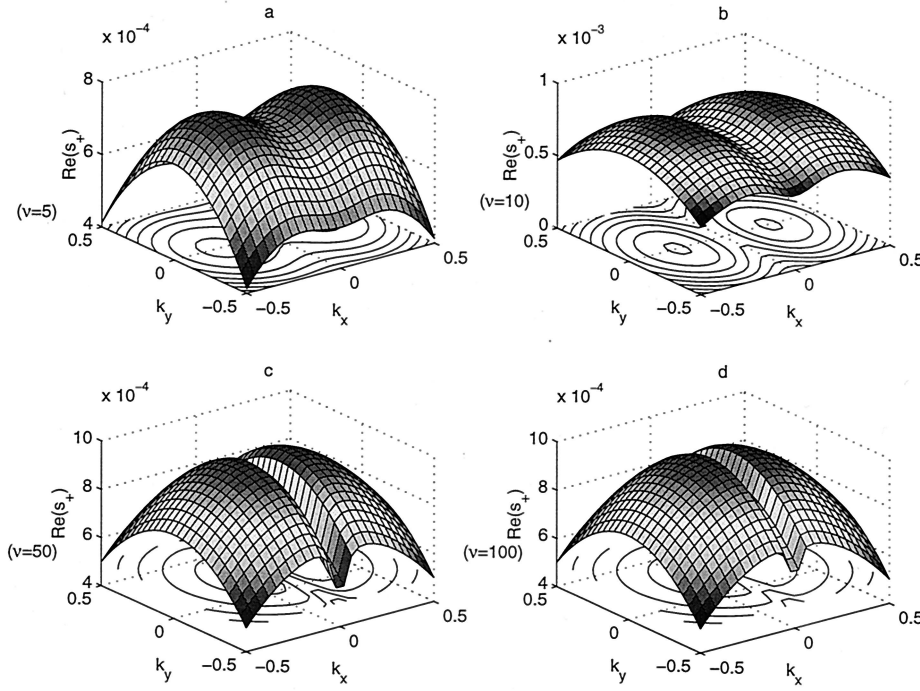


Figure A1. Two-dimensional dispersion relation for perturbations of the form $e^{i(k_x x + k_y y) + s t}$ to the equilibrium state ψ_0 given by Eq. (6) with $\alpha_s = 0.0009$, $\lambda = 0.001$, $\beta = 100$. Surfaces show the growth rate of the perturbation, $Re(s_+)$ (where s_+ is the one of two possible solutions for (a) that allows growth) versus wave-numbers k_x and k_y for (a) $v = 5$, (b) $v = 10$; (c) $v = 50$, (d) $v = 100$. Note the symmetry in k_x and that the least stable mode (location of largest $Re(s_+)$) always occurs at $k_y = 0$.

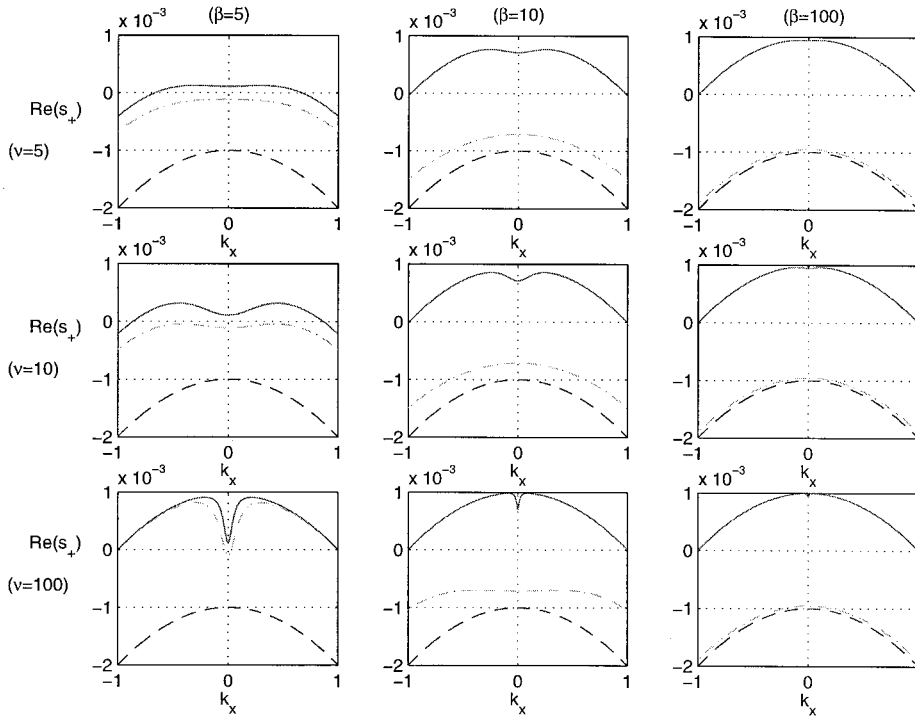


Figure A2. Growth rate $Re(s_+)$ versus wavenumber k for perturbations to the low solid-density quadratic root ψ_0^- (solid curves), to the high solid-density quadratic root, ψ_0^+ (dash-dot curves), and to the trivial steady state ψ_0^0 (dashed curves). Plots are for increasing reaction parameter, β from left to right ($\beta = 5, 10, 100$), and for increasing imposed pressure gradient, v , from top to bottom ($v = 5, 10, 100$).

$= 0$. Nonzero k_x implies that there is a finite wavelength that characterizes the fastest growth in x , while $k_y = 0$ implies that growth is uniform in y , perpendicular to the imposed pressure gradient. Thus, for further analysis of the dispersion relation,

we set $k_y = 0$ and analyze the system for spatial dependence in x .

We show for the one-dimensional case that growth is not sustained ($\max(Re(s)) < 0$) for the trivial case, and growth is sustained only over very

restricted ranges for the nutrient-limited steady state ψ_0^+ (Figure A2). For the solid-limited steady state, ψ_0^- , however, growth is sustained over a wide range of parameters. This result does not contradict our findings for sampled parameter ranges for the two-dimensional case. We thus examine only this consistently unstable root, ψ_0^- , in the main text.

REFERENCES

- Aharonov E, Whitehead JA, Kelemen PB, Spiegelman M. 1995. Channeling instability of upwelling melt in the mantle. *J Geophys Res* 100(10): 20433–20450.
- Bailyn M. 1994. A survey of thermodynamics. College Park, (MD): American Institute of Physics.
- Baker PA, Weber JN. 1975a. Coral growth rate: variation with depth. *Earth Planet Sci Lett* 27: 57–61.
- Baker PA, Weber JN. 1975b. Coral growth rate: variation with depth. *Phys Earth Planet Int* 10: 135–9.
- Bear J. 1988. Dynamics of fluids in porous media. Mineola (NY): Dover.
- Bercovici D, Ricard R, Schubert G. 2001. A two-phase model for compaction and damage. I. General theory. *J Geophys Res* 106: 8887–8906.
- Borowitzka MA. 1987. Calcification in algae: mechanisms and the role of metabolism. *CRC Crit Rev Plant Sci* 6 (1): 1–43.
- Chandrasekhar S. 1961. Hydrodynamic and hydromagnetic instability. New York: Oxford University Press.
- Drazin PG, Reid WH. 1989. Hydrodynamic stability. New York: Cambridge University Press.
- Gattuso JP, Allemand D, Frankignoulle M. 1999. Photosynthesis and calcification at cellular, organismal and community levels in coral reefs: a review of interactions and control by carbonate chemistry. *Am Zool* 39: 160–183.
- Goreau T. 1963. Calcium carbonate deposition by coralline algae and corals in relation to their roles as reef builders. *Ann NY Acad Sci* 109: 127–167.
- Graus RR, Macintyre IG. 1989. The zonation patterns of Caribbean coral reefs as controlled by wave and light energy input, bathymetric setting and reef morphology: computer simulation experiments. *Coral Reefs* 8:9–18.
- Helmuth BST, Sebens KP, Daniel TL. 1997. Morphological variation in coral aggregations: branch spacing and mass flux to coral tissues. *J Exp Mar Biol Ecol* 209: 233–259.
- HilleRisLambers R, Rietkerk M, Prins HHT, van den Bosch F, de Kroon H. 2001. Vegetation pattern formation in semi-arid grazing systems. *Ecology* 82: 50–61.
- Isa Y, Okazaki M. 1987. Some observations on the Ca^{++} -binding phospholipids from scleractinian coral skeletons. *Comp Biochem Physiol* 87B: 507–512.
- Jackson J. 1991. Adaptation and diversity of reef corals. *BioScience* 41(7): 475–482.
- Jain MK. 1984. Numerical solution of differential equations. New York: Wiley.
- Jupp DLB. 1985. Landsat based interpretation of the Cairns section of the Great Barrier Reef Marine Park. *CSIRO Div Water Nat Resou* 4:1–51.
- Kaandorp JA, Lowe CP, Frenkel D, Sloot P. 1996. Effect of nutrient diffusion and flow on coral morphology. *Phys Rev Lett* 77(11): 2328–2331.
- Kawaguti S, Sakumoto D. 1948. The effects of light on the calcium deposition of corals. *Bull Oceanogr Inst Taiwan* 4: 65–70.
- Lewis DH. 1973. The relevance of symbiosis to taxonomy and ecology, with particular reference to mutualistic symbioses and the exploitation of marginal habitats. In: Heywood VH, editor. *Taxonomy and ecology*. New York: Academic Press. p 151–172.
- Maxwell WGH. 1968. Atlas of the Great Barrier Reef. Amsterdam: Elsevier.
- Mistr S. 1999. Pattern formation in a reaction-advection-diffusion system with applications to coral reefs. [thesis]. Honolulu: University of Hawaii.
- Muscantine L. 1973. Nutrition of corals. In: *Biology and geology of coral reefs*. Jones OA, Endean R, editors. New York: Academic Press. p 77–116.
- Nicolis G. 1995. Introduction to nonlinear science. Cambridge (England): Cambridge University Press.
- Porter JW. 1976. Autotrophy, heterotrophy, and resource partitioning in Caribbean reef-building corals. *American Naturalist* 110: 731–742.
- Preece AL, Johnson CR. 1993. Recovery of model coral communities: complex behaviours from interaction of parameters operating at different spatial scales. In: *Complex systems: from biology to computation*. Green DG, Bossomaier T, editors. Amsterdam: IOS Press. p 69–81.
- Press W, Teukolsky S, Vetterling W, Flannery B. 1992. Numerical recipes in FORTRAN. New York: Cambridge University Press.
- Stumm W, Morgan JJ. 1981. Aquatic chemistry. 2nd ed. New York: Wiley.
- Turing A. 1952. Chemical basis of morphogenesis. In: Saunders PT, editor. *Morphogenesis*. Amsterdam: Elsevier.
- Veron JEN, Pichon J. 1976. Scleractinia of Eastern Australia. Part 1. Canberra: Australian Institute of Marine Science Monograph Series; vol. 1. Australian Government Publishing Service.
- Ware J, Smith SV, Reaka-Kudla ML. 1991. Coral reefs: sources or sinks of atmospheric CO_2 ? *Coral Reefs* 11: 127–130.
- Yonge CM. 1930. Studies on the physiology of corals. I. Feeding mechanisms and food. *Sci Rep Great Barrier Reef Expedition, 1928–29; Scientific Reports of the Great Barrier Reef Expedition, 1928–1929* 1: 13–57.